Physiologia Plantarum
An International Journal for Plant Biology

Physiologia Plantarum 2019 ISSN 0031-9317

Selective mineral transport barriers at *Cuscuta*-host infection sites

Frank Förste[a], Ioanna Mantouvalou[a], Birgit Kanngießer[a], Hagen Stosnach[b], Lena Anna-Maria Lachner[c], Karsten Fischer[c] and Kirsten Krause[c]*

[a]Institute for Optics and Atomic Physics, Technical University of Berlin, Berlin, 10623, Germany
[b]Bruker Nano GmbH, Berlin, 12489, Germany
[c]Department of Arctic and Marine Biology, The Arctic University of Norway UiT, Tromsø, 9019, Norway

Correspondence
*Corresponding author,
e-mail: kirsten.krause@uit.no

Received 13 June 2019;
revised 27 September 2019

doi:10.1111/ppl.13035

The uptake of inorganic nutrients by rootless parasitic plants, which depend on host connections for all nutrient supplies, is largely uncharted. Using X-ray fluorescence spectroscopy (XRF), we analyzed the element composition of macro- and micronutrients at infection sites of the parasitic angiosperm *Cuscuta reflexa* growing on hosts of the genus *Pelargonium*. Imaging methods combining XRF with 2-D or 3-D (confocal) microscopy show that most of the measured elements are present at similar concentrations in the parasite compared to the host. However, calcium and strontium levels drop pronouncedly at the host/parasite interface, and manganese appears to accumulate in the host tissue surrounding the interface. Chlorine is present in the haustorium at similar levels as in the host tissue but is decreased in the stem of the parasite. Thus, our observations indicate a restricted uptake of calcium, strontium, manganese and chlorine by the parasite. Xylem-mobile dyes, which can probe for xylem connectivity between host and parasite, provided evidence for an interspecies xylem flow, which in theory would be expected to carry all of the elements indiscriminately. We thus conclude that inorganic nutrient uptake by the parasite *Cuscuta* is regulated by specific selective barriers whose existence has evaded detection until now.

Introduction

Photosynthetic plants need many essential elements for their growth. These elements are taken up by the roots from the soil in the form of metal cations, anions or oxyanions. The macronutrients nitrogen (N), potassium (K), calcium (Ca), magnesium (Mg), phosphorus (P) and sulfur (S) are present in plant tissues in large amounts ($>50\,\mu mol\,g^{-1}$ dry weight [DW]; Maathuis 2009). The micronutrients boron (B), chlorine (Cl), copper (Cu), iron (Fe), manganese (Mn), molybdenum (Mo), nickel (Ni) and zinc (Zn) are required in much smaller amounts and are therefore found at much lower concentrations in plant tissues ($<5\,\mu mol\,g^{-1}$ DW, with the exception of Cl; Hänsch and Mendel 2009). All plants have to acquire appropriate amounts of each nutrient. Deficiencies in essential nutrients lead to inhibition of growth and to specific disorders. To avoid this, plants accumulate essential nutrients by active transport processes to much higher levels than those found in the surrounding soil. However, several nutritional minerals are toxic at elevated concentrations, entailing a duality of beneficial vs detrimental effects that necessitate the development of precisely tuned homeostatic networks for the uptake,

Abbreviations – DW, dry weight; MXRF, micro-X-ray fluorescence spectrometry; TXRF, total reflection X-ray fluorescence spectrometry; XRF, X-ray fluorescence spectrometry.

Frank Förste and Ioanna Mantouvalou contributed equally to this work.

transport and storage of nutrients (Hänsch and Mendel 2009). Long-distance transport from roots to other plant parts is mainly achieved through the transpiration stream in the xylem, while a re-distribution of many, but not all, elements between the different plant organs occurs via phloem transport (Conn and Gilliham 2010, Etienne et al. 2018). Within the organs, distribution is achieved via tissue- or cell-specific membrane transport processes and by membrane-lined intercellular tunnels called plasmodesmata.

Parasitic vines that belong to the angiosperm genus *Cuscuta* are rootless and consequently have no direct access to soil nutrients. The threadlike *Cuscuta* vines infect stems, petioles and pedicels of other plants (Fig. 1A–C) to cover their nutritional requirements. The connection between the two partners is formed by specialized, shoot-borne infection organs termed haustoria (Kuijt 1969, Dawson et al. 1994). These haustoria functionally replace the roots, which have been lost in the course of the parasite's evolution. Microscopic and electron microscopic studies as well as fluorescent tracers support the notion that there is a host-to-parasite continuum of the long-distance vascular system between both plants through the haustoria. This continuum is secured by different types of specialized cells that are summarized under the term 'feeding hyphae' and that develop at the tip of the haustorium (Doerr 1969, Vaughn 2003). The differentiation of these feeding hyphae depends on which host cell type they have established contact with. For example, xylem vessels of the host, which are comprised of dead tube-like cells, were observed to be intercepted by xylem-like hyphae that play a role in the redirection of water and minerals to the parasite (Christensen et al. 2003). On the other hand, amino acids, sugars, nucleotides and other organic molecules in the phloem sap are believed to be channeled to finger-like hyphae from phloem cells for long distance transport or from parenchymatous cells for short distance transport (Doerr 1972). Plasmodesmata that establish a symplastic continuum between neighboring cells were shown to exist between the *Cuscuta* hyphae and the host cells (Doerr 1969, Birschwilks et al. 2006, Vaughn 2006). Many *Cuscuta* species are fast-growing and form hundreds to thousands of haustoria on a single host (Fig. 1D).

Because of the enormous importance of nutrients for plant growth and also for human nutrition, the 'ionome', which corresponds to the total concentration (i.e. all forms) of elements in a sample (Conn and Gilliham 2010), has been studied extensively in crop plants. Many proteins involved in nutrient transport and storage, e.g. transcription factors, transporters and ion channels for membrane transport and metal binding

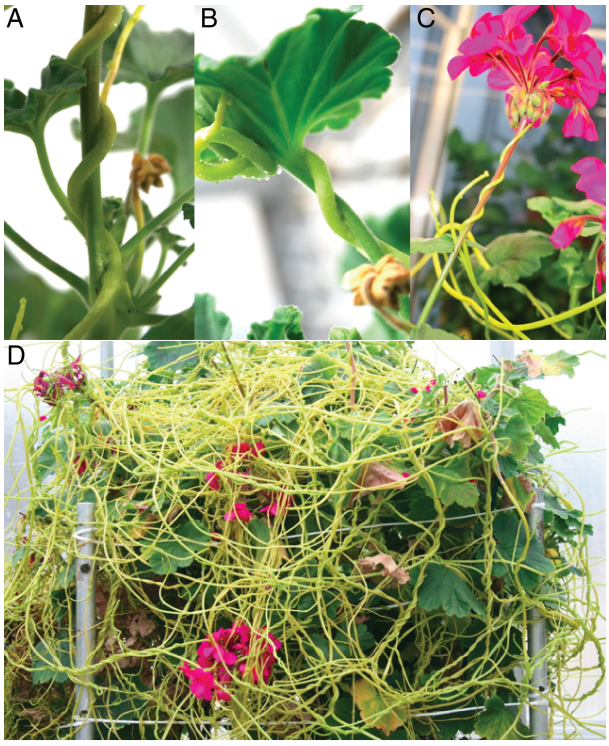

Fig. 1. Host–parasite interactions. (A–C) *Cuscuta reflexa* (giant dodder) infecting stems (A), petioles (B) and pedicels (C) of the ornamental plant *Pelargonium zonale*. (D) *C. reflexa* overgrowing *P. zonale* in a greenhouse.

proteins, have been identified and their physiological function has been determined in model plants (White and Broadley 2009, Etienne et al. 2018). Increasing the mineral concentrations in edible crops, e.g. is a big task in the strive for food security (White and Broadley 2009, Mantouvalou et al. 2017). An infection by *Cuscuta* species often causes severe crop yield losses (Costea and Tardif 2005), which in part seems to be related to the depletion of photosynthates in its hosts. A few studies have been published showing, surprisingly though, that *Cuscuta* does not deplete the host noticeably of its mineral elements (Wallace et al. 1978, Saric et al. 1991). The parasite was even shown to have much lower calcium levels than the plant supporting it. Sadly, three to four decades later, the knowledge around the transport fluxes of different compound classes from host to parasite and the uptake and distribution of inorganic nutrients at the *Cuscuta*-host border has not been refined despite a significant advancement of the technical possibilities to study macro- and microelement content and distribution.

Ionomics (the simultaneous measurement of the elemental composition by high-throughput elemental analysis technologies; Salt et al. 2008) is performed by X-ray

fluorescence spectroscopy (XRF). This is an elemental detection technique, which relies on the principle that atoms are excited with ionizing X-ray radiation and the resulting X-ray fluorescence is detected with an energy-dispersive detector (Beckhoff et al. 2007). Owing to the distinctive energy levels in atoms, the X-ray fluorescence spectrum is characteristic for each element, thus, elemental information can be obtained. Quantification of elemental composition is possible by linking the measured X-ray fluorescence intensity to the concentration of the elements either through the measurement of similar reference samples or through the use of the fundamental parameter approach (van Grieken and Markowicz 2001). By using X-ray optics, the exciting radiation can be focused onto a micrometer-sized spot, thereby resolving the elemental distribution within a sample (Haschke and Haller 2003, Havrilla and Miller 2004). Due to the penetrating nature of X-rays, three-dimensionally resolved elemental imaging can be achieved when utilizing two X-ray optics in a confocal arrangement (Mantouvalou et al. 2012). For biological specimens, the main matrix elements (C, H, O) are not typically accessible with XRF, thus elemental imaging is especially suited for the distribution analysis of minerals and metallic trace elements. Generally, the low density of the material and the low concentrations of the fluorescence elements lead to a low fluorescence yield.

We present here the first space-resolved study of the element distribution in a system that involves two interacting plants, i.e. *Cuscuta reflexa – Pelargonium zonale* infection sites and the surrounding stem sections. With XRF, we show that the parasite does not indiscriminately absorb all of the hosts' nutrients but, instead, appears to specifically regulate the uptake of calcium, strontium, chlorine and manganese.

Materials and methods

Plant material and growth conditions

The parasite *Cuscuta reflexa* ROXB. and the host *Pelargonium zonale* 'Kardinal' were originally obtained from the Botanical Garden of the Christian-Albrechts-University in Kiel. Host and parasite were cultivated together under continuous illumination in daylight chambers supplemented with additional neon lights at the Phytotron of the University of Tromsø, Norway. Growth rooms had a constant temperature of 21°C. Host plants were propagated by taking cuttings from uninfected plants. The parasite was propagated by placing apical shoot segments of approximately 20 cm in water-filled tubes in the pots of the host and allowed to infect the hosts as described (Krause et al. 2018). All experiments were performed on hosts that were infected at least 4 weeks prior to sampling.

Sample collection and preparation

Infection sites closest to the apical shoot tips of *C. reflexa* were used for analysis. The selection of these sites was guided by the tell-tale signs that a feeding connection was established (resumed growth of the shoot above the infection site and side branch production [Olsen et al. 2016]). The distance between infection sites and shoot tips of the parasite was kept within a range of 15 to 25 cm. To avoid contamination from the equipment, samples were handled only with plastic forceps and cut only with ceramic knives or ceramic razor blades. For total reflection XRF (TXRF) measurements with the Picofox instrument, 3–6 mm shoot sections of parasite and host, above and below the infection site, were carefully cut with a ceramic knife, weighed and placed in plastic containers. For TXRF measurements with the S4 T-Star, shoot tips with 2–3 branching nodes (10–12 mm) were collected. For micro X-ray fluorescence spectrometry (MXRF), 2 mm sections (+/− 0.5 mm) of an infection site were cut with a ceramic knife and placed on a piece of carbon tape inside a plastic tube. The plant material was weighed, flash-frozen in liquid nitrogen and subsequently freeze-dried for 24 h under 5 mTorr vacuum. The freeze-dried samples were weighed again and kept protected from moisture at room temperature until they were scanned.

S2 Picofox measurements

Five milliter ultrapure water, 10 µl of a gallium standard solution (1 g l^{-1}) and 10 yttrium-coated ceramic balls (diameter 2 mm) were added to the sample tubes containing fresh pre-weighed plant samples. The samples were placed in an automatic homogenizer (Omni Bead Ruptor 24, Omnilab International Inc.) and homogenized with the following settings: speed (6 m s^{-1}), number of cycles (2), homogenization time (35 s), dwell time between cycles (10 s). 10 µl of the homogenate was transferred onto siliconised quartz glass sample carriers and dried in vacuum. The instrument (S2 Picofox, Bruker Nano GmbH) used for the measurements was equipped with a 50 W Mo-tube, operated at 50 kV/600 µA, and a 30-mm^2 silicon drift detector. Measurement times were 1000 s. As this technique is nearly free from any matrix effects, the concentration of all detected elements is directly calculated based on the measured fluorescence intensities and the concentration of the internal standard element. To convert the concentrations to milligram per kilogram dry weight, an average ratio of fresh weight to

dry weight of 13.3:1 (as determined by weighing before and after freeze-drying) was applied.

S4 T-Star measurements

Pre-weighed freeze-dried plant material was homogenized in 0.5 ml ultrapure water supplemented with 10 µl of a gallium standard solution (10 mg l^{-1}) and 3 yttrium-coated ceramic balls (diameter 3 mm) first in an ultrasonic bath (3 min) and then in an automatic benchtop mill (Retsch MM400; 3 min at 30 Hz). 10 µl of the homogenate was transferred onto siliconised quartz glass sample carriers and dried in vacuum. The instrument (S4 T-Star, Bruker Nano GmbH) was operated with Mo-K excitation at 50 kV/1000 µA for 1000 s.

MXRF and confocal MXRF

The commercial MXRF spectrometer (Bruker M4 tornado) was equipped with a Rh microfocus X-ray tube, a polycapillary lens to focus the radiation and a SDD detector (Lachmann et al. 2016). In front of a second SDD a second polycapillary lens was mounted perpendicular to the first, thus creating a confocal MXRF setup which enabled three-dimensional-resolved measurements with a resolution of 30 µm at Fe Kα (Mantouvalou et al. 2017). A fisheye camera with two magnification stages (10× and 100×) was used for positioning of the sample. The sample stage could be moved in three directions with a maximal speed of 100 mm s^{-1}. In the normal configuration, the sample environment can be evacuated to pre-vacuum conditions (20 mbar). For the analysis of cryogenic samples, the spectrometer was equipped with a Cryojet from Oxford instruments. The snout of the jet is inserted through an unoccupied flange at the measuring head and positioned for a local freezing of a sample at the measuring position. The sample temperature could be monitored. The whole sample environment was flushed with nitrogen to prevent icing of the samples during transfer. All measurements were performed with a tube voltage and current of 50 kV and 600 µA, respectively. Measurement times and pixel sizes are described in the figure legends or in the main text.

For the high-resolution confocal scan, a voxel (3D pixel) size of 50 µm and a dwelling time of 130 s per voxel was used.

Visualization and quantification of MXRF data

The Esprit software from Bruker Nano was used for the visualization of the elemental images in Figs. 3, 4A, 5, S3 and S4. For this purpose, the fast deconvolution setting was used, yielding images of the distribution of the net peak intensities of the fluorescence peaks of the respective elements. For an adapted visualization, the contrast was set either to maximal contrast or to an optimal differentiation between host, haustorium and parasite.

The element distributions of the confocal measurement in Fig. 4B and video supplement were generated through deconvolution and absorption-correction (Mantouvalou et al. 2017) by in-house software. The compound visualization in Fig. 4B was created with the software Tomviz using the contour visualization method.

For the charts shown in Fig. 5, sum spectra of the circular regions of the transect consisting of approximately 16 pixels were generated with the Esprit software. The spectra were normalized to the elastically scattered Rh Kα peak originating from the excitation spectrum in order to render a comparison feasible. Subsequently, the spectra were deconvolved and the net peak intensities of the respective fluorescence lines plotted against the number of the region with OriginPro 8.5.1. Similarly, the graphs in Fig. S2A,B were prepared by normalizing the sum spectra of the complete samples.

Xylem transport analysis

Infected pedicels were cut 6–8 cm below the infection site and placed immediately in a ink:tap water (1:10) mix. Meanwhile, the infecting shoot of the parasite was not severed and remained connected to the rest of the *C. reflexa* plant. The infection site was hand-cut after 24 h and inspected with a stereomicroscope equipped with a color camera.

Immunolabeling of Ca-crosslinked pectin

Infection sites were fixed in Farmer's fixative (Ethanol: Glacial acetic acid in a ratio of 3:1 [v:v]) under vacuum for 2 × 15 min and an additional 6-24 h under ambient pressure at 4°C, dehydrated in an ethanol series (75, 85, 95 and 100% [v/v]) with transfer every 2 h. Half of the volume of 100% EtOH was removed, the sample incubated at 38°C for 10 min and molten Steedman's wax added to achieve a 1:1 mixture. After a 12-h incubation at 38°C, the mixture was exchanged with 100% molten wax 3 times with 2 h intervals keeping it at 38°C. After letting the wax solidify at RT (for 24 h or more before cutting) cross-sections of 10–12 µm thickness were cut with a microtome, mounted on poly-L-lysine-coated microscopy slides and dried over night at 32°C. Prior to immunolabeling, slides were dewaxed by adding 100% EtOH and warming the slides to 32°C. Sections were blocked with 5% milk powder dissolved in T/Ca/S buffer (Tris-HCl 20 mM pH8.2, $CaCl_2$ 0.5 mM, NaCl 150 mM)

for at least 30 min at RT and then incubated for 90 min with the 2F4 Anti-homogalacturonan antibody (PPG1-2F4, Plant Probes) (Liners et al. 1989) diluted 1:25 in T/Ca/S buffer as specified by the producer.

After three 5-min washes with T/Ca/S buffer, followed by a 1-h incubation in the dark in a 1:1000 dilution of the secondary antibody (Alexa Fluor 555 goat anti-mouse) in T/Ca/S buffer and three further 5-min washes, the sections were mounted on microscopy slides using a drop of citifluor AF1 mounting medium (Glycerol/PBS) and stored in the dark at 4°C until viewing. The immunolabeling was investigated using fluorescence microscopy. The primary antibody was omitted in controls for autofluorescence background and unspecific binding of the secondary antibody.

Results

Calcium, manganese and chlorine are strongly reduced in *C. reflexa* compared to its host *P. zonale*

It has been an unsolved issue whether the diversion of nutrients from the host to the parasite might lead to a change in element composition around the infection site in either of the partners. To investigate this, we first measured the total content of major mineral nutrients and trace elements in stems of both interaction partners, above and below infection sites, using TXRF (Klockenkämper and van Bohlen 2015). With this particularly sensitive variant of XRF, elemental concentrations of homogenized specimens down to the parts-per-billion level can be derived. This analysis revealed that the sites above and below the host–parasite connection in each interaction partner were very similar with regard to almost all elemental concentrations (Fig. 2) and that they matched the concentration range measured in other plants (Watanabe et al. 2007). The same is true for most nutrients when comparing the tissue of the host and the parasite. Most of the macroelements (P, S, K) and microelements (Fe, Cu, Zn) showed the same concentration in both plants or, as in case of the non-essential rubidium, they were slightly more abundant in *C. reflexa* (10–20%). None of the elements, however, accumulated to significantly higher values (increase of more than 50%) in the parasite compared to the host plant. However, several elements showed a clear decrease in the tissue of the parasite. These include Cl (~50% average decrease), Ca (>90% average decrease), Mn (~75% average decrease) as well as the non-essential or toxic trace elements bromine (Br) and strontium (Sr) (80–90% average decrease; Fig. 2). These differences lead to different relative ratios of the elements in the host and the parasite. While in *P. zonale*, the macroelement concentrations decreased in the order $K > Ca > P \cong Cl > S$, the order in *C. reflexa* was $K > P > S \cong Cl > Ca$. In apical shoot tips, the absolute quantities were in the same range and the relative order differed only slightly due to a shift of the chloride abundance ($K > P > S > Cl \cong Ca$). No indication was obtained for an accumulation of any element except Mn in the apical tips of growing shoots (Fig. S1). This suggested that selective exclusion mechanisms of minerals might exist at the host–parasite border, calling for a spatially resolved analysis of the host–parasite interfaces at the infection sites themselves.

Spatially resolved element patterns in situ can be achieved by MXRF

MXRF is able to capture changes in element distribution non-invasively with a high lateral spatial accuracy and was chosen for this task. To obtain the desired resolution, measuring times of 3 h and more had to be applied, necessitating cryofixation of the samples to avoid dehydration and migration of mobile elements (Gianoncelli et al. 2015, de Carvalho et al. 2018). Samples with a thickness of 2 mm proved to be optimal for our measurements since they provided sufficient fluorescence intensities while simultaneously keeping low the occurrence of artifacts due to tissue inhomogeneity.

Initially, MXRF images of infection site cross-sections were compared between samples that were either flash-frozen and kept frozen under a stream of nitrogen gas applied with a CryoJet (Oxford Instruments) during the measurements or that were freeze-dried prior to the measurements. It was found that the distribution of the elements was not influenced by the preparation method, implying that in the probed lateral dimension scale and for the investigated samples no significant movement of mobile elements during the freeze-drying process took place. However, with the exception of chlorine, the intensities of the elemental spectra were often higher in freeze-dried samples (Fig. S2) due to the elimination of scattering from water or ice. All following MXRF data were therefore obtained on freeze-dried cross-sections.

Element content differences between host and parasite are independent of the type of host stem and the species

C. reflexa indiscriminately infects the main stems, petioles and pedicels of its hosts. While petioles connect source tissue (the leaves) to the main shoot, pedicels supply a sink tissue (the flowers), so the relative amounts of the elements could deviate in these tissues. To determine whether the tissue type that is infected has an impact

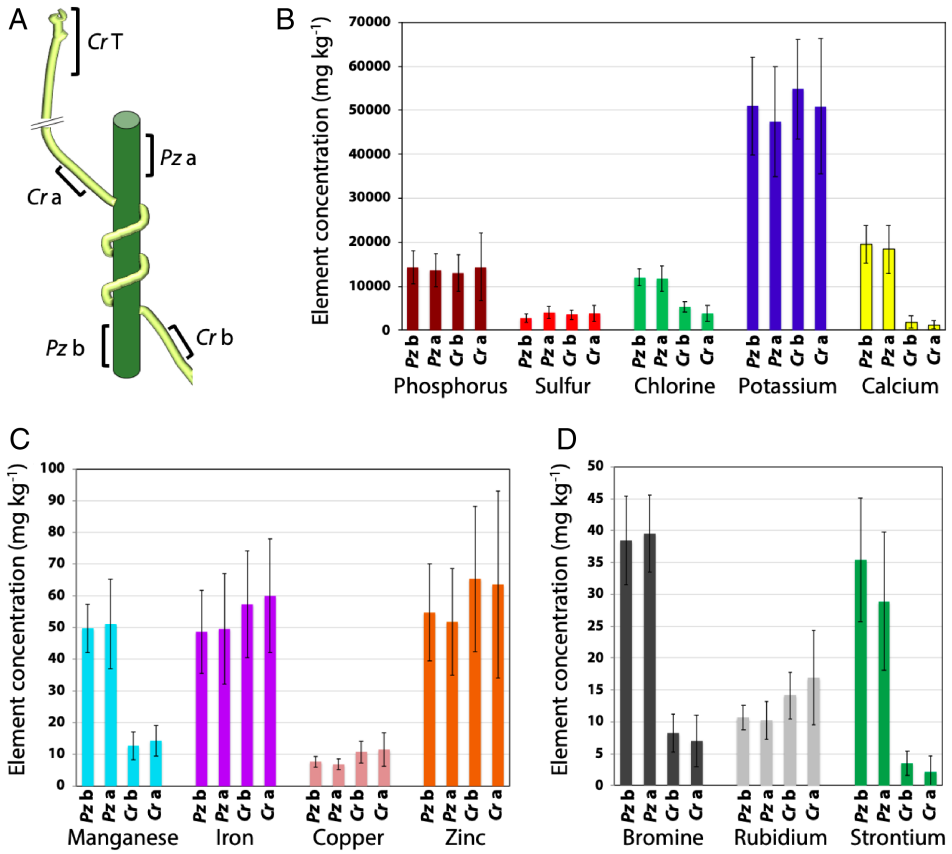

Fig. 2. Element composition of host and parasite stem extracts below and above the infection site. (A) Schematic representation of the sample sites. *Cr* a and *Cr* b refer to sample sites in the stems of the parasite, *Cuscuta reflexa*, above and below the infection sites, respectively. *Pz* a and *Pz* b refer to sites in the stems of the host, *Pelargonium zonale*, above and below the infection sites, respectively. Apical tips of *C. reflexa* (*Cr* T) were between 15 and 25 cm away from the infection site. The average element composition of shoot tips is shown in Fig. S1. (B–D) Macronutrient (B), micronutrient (C) and non-essential (D) element concentrations are given in mg/kg dry weight (mean ± SE; n = 15). Samples were taken in groups of three on five different days over a period of 2 weeks. All samples are derived from a set of four infected *P. zonale* plants.

on the elemental distribution patterns within the infection sites, we compared cross-sections through infection sites on each of them. This survey revealed that the intensity of all elemental spectra was similar in the three stem types (Fig. S2). Likewise, relative ratios of the elements between host and parasite were not influenced by the stem type, and only small differences were observed in the distribution within each partner (Figs 3 and S3). These differences are mostly connected to the organization of the vascular tissue in the host and are most evident in the pedicels. The distribution between host and parasite showed the same tendential differences when another *Pelargonium* species (*P. citriodorum*, lemon-scented *Pelargonium*) was used as host (Fig. S2), with the notable exception of Cl, which was found to be higher in *C. reflexa* when attached to *P. citriodorum*.

Discrimination against calcium, manganese and chlorine between *C. reflexa* and *P. zonale* occurs at two different barriers

MXRF-scanned cross-sections of *C. reflexa*-*P. zonale* petiole infection sites confirmed that the macronutrients P and K and the micronutrient Zn were present at similar concentrations in host and parasite, although local fluctuations were recorded. Cl, Ca and Sr were clearly reduced in *C. reflexa* (Fig. 4A), confirming the TXRF measurements. The measured concentrations of sulfur were more inconsistent and showed a decrease in parasite shoots infecting *P. zonale* petioles (Fig. 4A), and an increase in stem- and pedicel-infecting *C. reflexa* shoots (Figs S3 and S4). For the element Mn, a diffuse signal throughout the host stem was observed that was more intensive than the signals in the parasite. Additionally, striking accumulations around the haustorium were visible, which were not observed with any of the other elements (Fig. 4A). To get a more accurate picture of the distribution of the elements in the different regions of an infection site, a high-resolution confocal scan of the endophytic haustorium and its surrounding tissue (volume of 1550 µm × 450 µm × 1000 µm) was performed (Fig. 4B and Movie S1). This confocal approach clearly showed that K, Ca and Mn each have a very distinct distribution pattern: while the haustorium is depleted for Ca and Mn, K is slightly enriched here. A distinct thin layer of Mn engulfing the haustorium is also visible (Movie S1).

In addition, for the 2D scans of two separate infection sites, 22 and 24 punctate sum spectra, respectively,

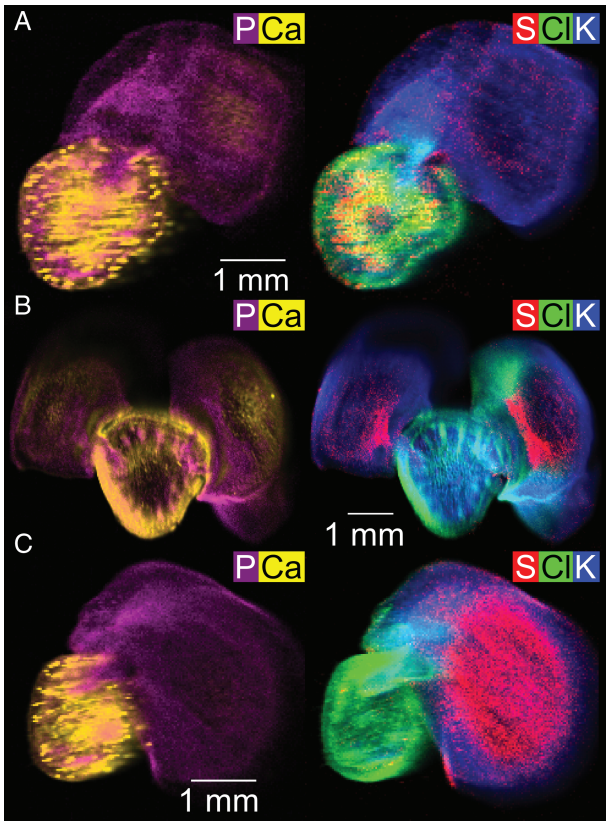

Fig. 3. Elemental distribution in infection sites. (A–C) Overlays of elemental patterns at infection sites on stems (A), pedicles (B) and petioles (C). The intensities for the P (purple), Ca (yellow), S (red), Cl (green) and K (blue) fluorescence peaks of the XRF spectra were derived with integration times of 3 s (for A), 3.85 s (for B) and 5.6 s (for C) per pixel, respectively, and a pixel size of 30 μm. The scaling of the intensity was chosen for an optimal visual differentiation of the different tissues. The intensities for each element are shown in numbers in Fig. S2. Individual pictures for each element are shown in Fig. S3. The relevant part of the sum spectra of the three measurements is shown in Fig. S2C.

were obtained (see Fig. S2C for an example) for spots placed along a transect from host epidermis through the middle of the haustorium into the parasite to its epidermis (Fig. 5A,B). The plotted intensities in Fig. 5C–F show that P shows on average the most stable distribution with similar intensities in all tissues. K showed an intensity peak at the top of the haustorium, where the signals were up to twice as high as in the remaining tissue, while fluorescence peaks from Ca and Sr, on the other hand, decreased sharply at the border between host and parasite, continuing to be low in the parasite stem with only a minor accumulation in the pith of *C. reflexa* (Fig. 5C,D). Although the values for S were on average a bit lower in the parasite (including its haustorium), the differences were by far not as drastic as for Ca and Sr Signals specific for Cl, in stark contrast, stayed at host levels throughout the haustorium and only dropped sharply in the *C. reflexa* stem, where they leveled out at ~10% of the values seen in the host (Fig. 5E,F).

Reduced Ca levels in *C. reflexa* are not due to a lack in xylem connections

The long-distance transport of Ca in plants is unidirectional from roots to shoots and leaves and only mediated by the xylem stream and there is overwhelming evidence showing that calcium is not translocated in the sieve tubes of the phloem (e.g., White and Broadley 2009, Conn and Gilliham 2010, Gilliham et al. 2011, Etienne et al. 2018). Although there is good microscopic evidence for the formation of xylem bridges between *C. reflexa* and *P. zonale*, we wanted to investigate whether the drop in Ca concentrations in *C. reflexa* could nevertheless reflect an inability to take up substances from the xylem. To this end, we placed infected host pedicels into tap water supplemented with blue ink for 24–36 h and hand-sectioned infection sites for subsequent microscopical analysis. The dark blue ink could be easily observed in the host xylem and was clearly transferred into the *C. reflexa* haustorium (Fig. 6). This simple experiment confirms that functional xylem connections do exist between *P. zonale* and *C. reflexa* and that the exclusion of Ca at the border of the haustorium must be due to some type of selective barrier.

Reduced Ca levels in *C. reflexa* do not appear to impact the parasites' ability to cross-link pectin

To analyze whether differences of calcium ions cross-linked in the cell walls of *C. reflexa* might explain its low Ca level, we used the monoclonal antibody 2F4 which binds to Ca^{2+}-crosslinked pectin (Rydahl et al. 2018). Immunolabeling of thin sections of fixed and embedded infection sites of *C. reflexa* on *P. zonale* showed no significant difference in the labelling intensity of cell walls between host and parasite (Fig. S5).

Discussion

A few studies on elemental composition in *Cuscuta* were performed already several decades ago. They reported on the levels of five elements (N, P, K, Ca and Mg) in *C. reflexa* infecting five different genotypes of *P. zonale* (Saric et al. 1991) as well as in *C. nevadensis* grown on eight different host species (Wallace et al. 1978). Owing to limitations of the measuring techniques used back then, only one element at a time could be measured and the tissue was used up in the process, aggravating

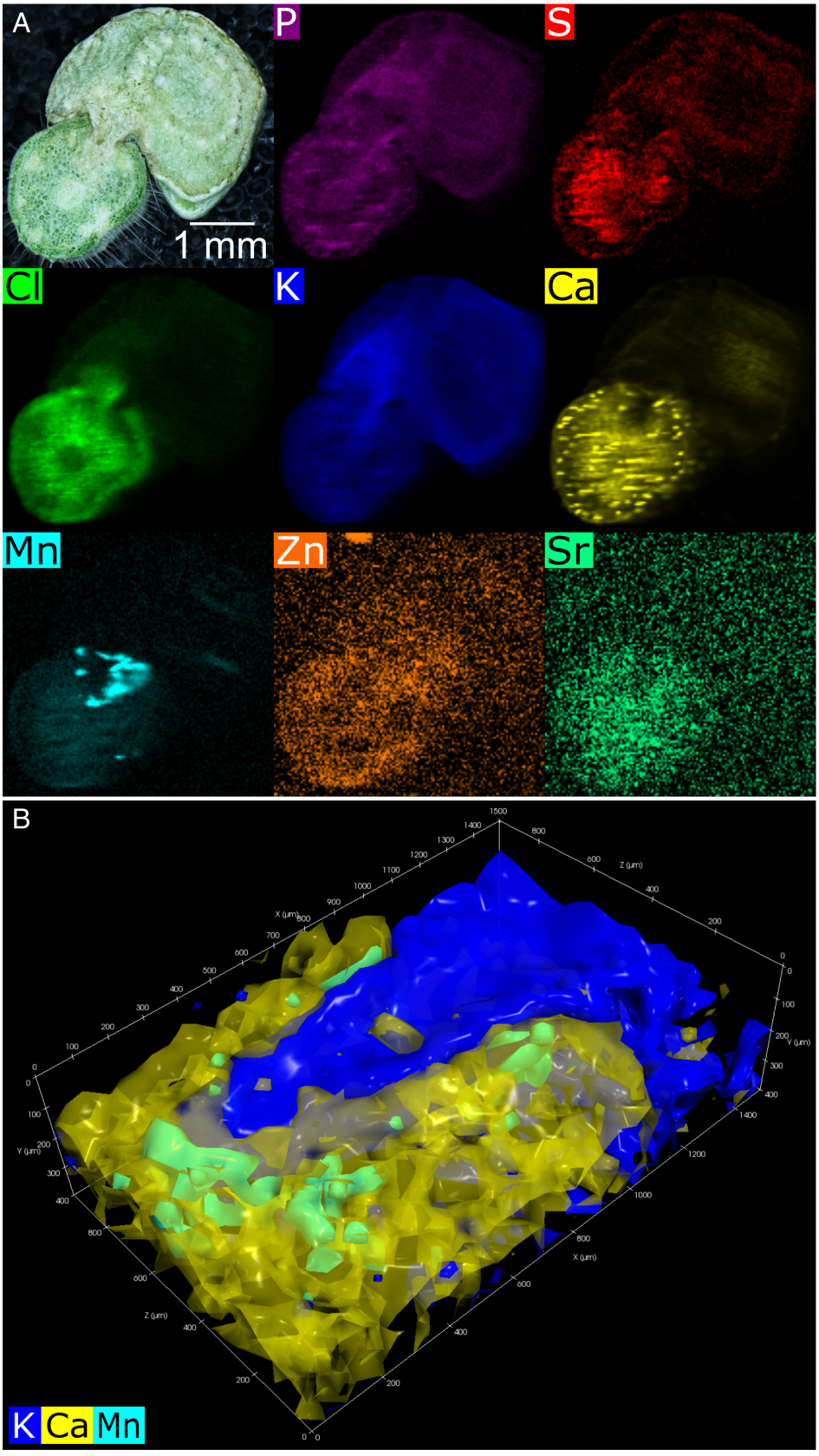

Fig. 4. Elemental distribution maps of a *Cuscuta reflexa* infection site on a representative *Pelargonium zonale* petiole. (A) Two-dimensional scan conducted with 30 µm pixel size and 3 s measuring time per pixel. Intensity distributions are scaled to maximal contrast. Further scans for petioles of the same and another species are shown in Fig. S4. (B) Confocal (three-dimensional) scan of the haustorium. The measurements were conducted in a volume of 1550 × 450 × 1000 µm using scanning steps of 50 µm and a measuring time of 130 s per voxel. *Cr*, *Cuscuta reflexa*; *Pz*, *Pelargonium zonale*. A video with rotating views of the scanned area is provided as Movie S1.

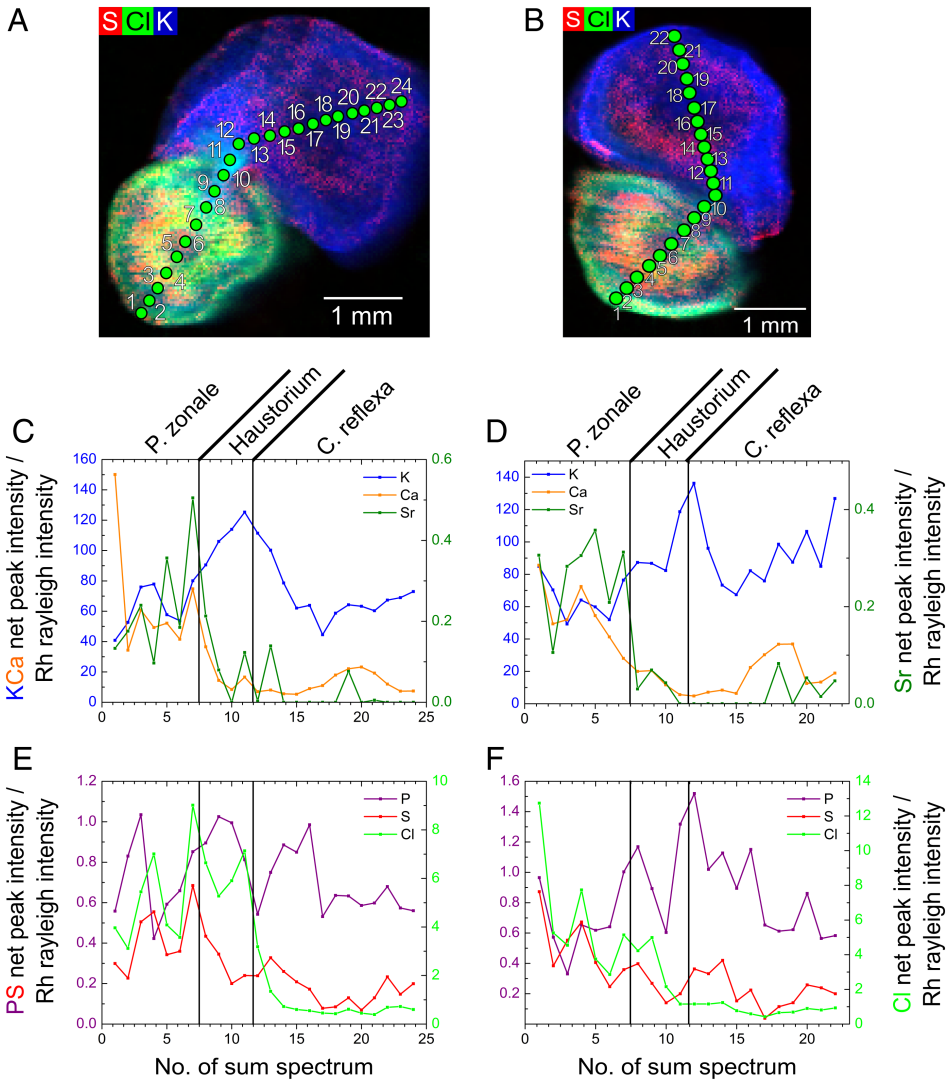

Fig. 5. Elemental distribution along a median transect in two independent infection sites on *Pelargonium zonale* petioles. (A-B) In the elemental images 24 (A) and 22 spectra (B), respectively, were generated by summing the intensity of approximately 16 pixels for each spectrum at the positions marked with the green circles. (C) Net peak intensity values for the K fluorescence lines of K, Ca and Sr normalized to the Rh Rayleigh scattering signal for each green circle shown in (A). (D) Same as (C) but representing green circles in (B). (E) Net peak intensity values for the K fluorescence lines of P, S and Cl normalized to the Rh Rayleigh scattering signal for each green circle shown in (A). (F) Same as (E) but representing green circles in (B).

accurate ratio comparisons. Also, the needed sample volumes limited the spatial resolution of these studies significantly. Modern XRF techniques, such as TXRF or MXRF, allow to do parallel measurements with the same sample for a wide range of elements, including those present in minute amounts (Andresen et al. 2018), which increases the accuracy of pattern comparisons also in the micronutrient range of elements. These techniques have been applied to many single plants, but not yet to a system where two plants interact with each other. By presenting XRF-based data on the *Cuscuta-Pelargonium* interaction system, our study is the first to show a detailed spatial analysis of mineral nutrient uptake at the interface between a shoot parasitic plant species and its compatible host.

While, surprisingly, we failed to find evidence for a pronounced accumulation of any macro- or microelement in the parasite compared to the host plant, we did observe sharp reductions in the Cl, Mn and Ca contents, in addition to 80–90% reductions of non-essential or toxic elements such as Br and Sr. The relative patterns of all elements resembled each other in all parts of the stems, whether measured around the infection sites or in the shoot tips. They were also not changed when the parasite was connected to a stem supporting a sink tissue (flowers), as opposed to a source tissue (leaf). The observed concentrations of all elements in *C. reflexa* are generally in accordance with the earlier mentioned studies (Wallace et al. 1978, Saric et al. 1991) and reveal that the parasite does not invest much energy into their (pronounced) accumulation or storage. It underlines the strict dependence of the parasite on its hosts despite the parasite's ability to photosynthesize (van der Kooij et al. 2000), and

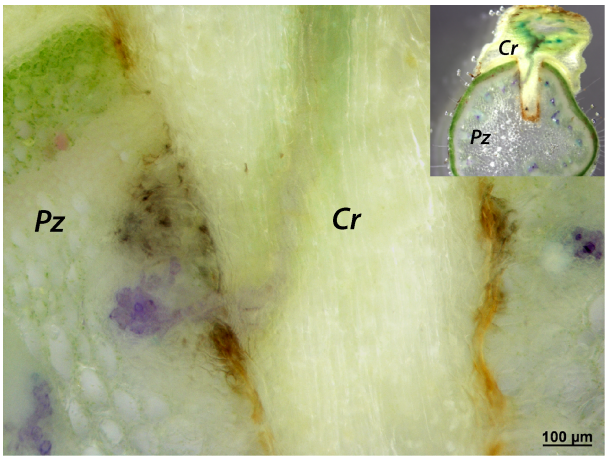

Fig. 6. Xylem connections between *Cuscuta reflexa* (*Cr*) and *Pelargonium zonale* (*Pz*). Hand-sectioned cross-section showing the host/haustorium interface of an infected host pedicel watered with blue Chinese ink (diluted 1:10 in water). The inset in the top right corner shows the entire infection site with the parasite on top of the host.

explains the limited survival time of *C. reflexa* shoots in the absence of a host. The strong depletion of some elements suggested the existence of one or more filtering mechanism(s) that hinder the import of these nutrients into the parasite. For Ca, Mn and Sr, MXRF provided evidence for a tentative selectivity barrier at the host–parasite interface and for a second tentative gateway that seems to control the uptake of Cl between the endophytic and exophytic tissue of *C. reflexa*. The identical distribution of Ca^{2+} and Sr^{2+} ions at the infection sites can be explained by the lack of discrimination of many Ca transport systems between these two ions and is corroborated by the fact that Sr can be used as analog for Ca to label the routes it travels through plants (Storey and Leigh 2004). In the following, the physiological role of the three depleted nutritional elements, Cl, Mn and Ca, and the putative implications of their lower abundance in *Cuscuta* shall be discussed.

Chlorine

Chloride (Cl^-), the anion of the element chlorine, is required, among others, in the oxygen-evolving complex of photosystem II (PSII) (Wege et al. 2017) and is thus essential for photosynthetic plants. However, only micromolar concentrations are required to avoid Cl-deficiency symptoms like chlorosis. The levels found in *C. reflexa* are several times higher than what is necessary for photosystem II function so that the very low photosynthesis rates in *C. reflexa* (van der Kooij et al. 2000) cannot be the reason for the low Cl accumulation rates.

It was reported that the macronutrient concentrations at which the Cl^- anion is present can act as a charge balance of essential cations such as K^+ and Ca^{2+} and as an osmoticum to regulate cell turgor (Franco-Navarro et al. 2016, Raven 2017, Wege et al. 2017). It also regulates stomatal conductance, which has an impact on water-use efficiency (Franco-Navarro et al. 2016). These attributes make Cl a beneficial macronutrient (Geilfus 2018) and may explain its observed distribution pattern in *C. reflexa*. On one hand, the haustorium with its rapid and invasive growth requires a high turgor pressure, which again calls for high Cl concentrations. On the other hand, *C. reflexa* stems lack leaves for transpiration and their stems have very few stomata, reducing transpiration and therefore the need of Cl to maintain their water balance. How the differential depletion of Cl is achieved in the parasite remains to be answered.

Manganese

Mn was the only element found to accumulate moderately in shoot tips, so that its depletion in tissue close to the infection site may be a result of low uptake rates paired with a relocation within the parasite. Mn is bound to more than 30 proteins as a catalytically active metal, among others in the water-splitting apparatus of photosystem II (Hänsch and Mendel 2009). It is required for photosynthesis, carbohydrate metabolism, and lipid and lignin biosynthesis. Photosynthetic activity was slightly higher in the shoot tips (van der Kooij et al. 2000), which could explain the moderate accumulation of Mn there. Whether *Cuscuta* restricts the uptake of Mn as part of a control mechanism to avoid Mn phytotoxicity symptoms that are known from crops (Fernando and Lynch 2015) is currently unknown.

Calcium

Ca is a macronutrient whose levels can differ by a factor of 50 between different species (from 1 to 50 mg Ca g^{-1} dry matter; Watanabe et al. 2007, Neugebauer et al. 2018, White et al. 2018) and in different tissues of the same plant. Ca participates in numerous processes involving nearly all aspects of plant development (Hepler 2005). The extremely low concentrations at which Ca is needed in the cytoplasm (≤ 0.1 µM) are reached even in *C. reflexa*, but the situation is different in the apoplast, where more than 50% of the total cellular Ca are present in its charged form (as the Ca^{2+} ion). Ca is particularly found in the primary cell wall, middle lamella and at the outer face of the plasma membrane. Its removal rapidly compromises membrane integrity (Hepler and

Winship 2010, de Freitas et al. 2012) and impacts the cross-linking of pectic homogalacturonan (HG), thereby jeopardizing the structure and the rigidity of the pectic cell wall fraction (Willats et al. 2001, Bosch and Hepler 2005, Hongo et al. 2012).

With less than 2 mg g^{-1} dry matter, the Ca levels in *Cuscuta* tissues proximal to an infection site and in distal shoot tips are decidedly at the lowest end of this spectrum and are only matched by Poales (2–10 mg g^{-1} dry matter). Here, the low Ca levels are a result of the low pectin content of their cell walls (Watanabe et al. 2007, Neugebauer et al. 2018, White et al. 2018). Immunological analyses of the cell wall composition of *C. reflexa*, however, revealed no apparent differences in Ca-crosslinked pectins (Johnsen et al. 2015 and Fig. S5), but this tentative conclusion should be viewed with caution since the antibody used to detect Ca-crosslinked pectins requires Ca in the binding buffer in order to work, and this could mask a Ca-deficiency in the tissue. Future work will have to find answers to imposing question like whether Ca was replaced by other ions in the apoplast and in other Ca-rich organelles in *Cuscuta* or how Ca deficiency symptoms at these far-below-average Ca levels are avoided.

Transport processes as the basis for element uptake selectivity

Long distance transport of mineral nutrients in the xylem of plants is driven strongly by the transpiration stream but many, though not all, elements can also be remobilized and redistributed by transport in the phloem, for example from leaves to roots, fruits (Etienne et al. 2018) or to a parasite. Cl^- is highly mobile both in xylem and phloem and should in theory experience no restrictions in its uptake, and yet the parasite shows lower levels of Cl. With the Cl concentrations in the haustorium matching that of the surrounding host tissue, one explanation is that the element is retained actively in the haustorium to maintain turgor pressure (see above) by reducing transfer from there to the *Cuscuta* stem. This is assumed to be particularly important in the young growing haustoria that were analyzed in our study. A theoretical alternative to explain the uneven Cl distribution is that it is depleted from the stems close to infection sites through rapid transport into other parts of the parasite. That the growing shoot tip could be a sink for Cl was not substantiated in this study, but it is still possible that older parts of the parasite could accumulate Cl. A search in the sequence databases for *Cuscuta* revealed that the parasite contains homologs for almost all Cl^- transporters and channels found in autotrophic plants (data not shown). However, it should be pointed out that these transporters belong to gene families for which the specific functions have not been dissected in detail. Functional studies, protein localization and spatially-resolved expression patterns of all putative Cl^- transporter candidates should be investigated before the basis for the differential Cl distribution can be explained.

Strikingly, the two essential elements Mn and Ca, which show the largest reduction in their concentration in *C. reflexa* compared to the host, have low (Mn) or no (Ca) mobility in the phloem. These elements can therefore enter *Cuscuta* mainly, or only, via the xylem bridge between the two species. Seeds and fruits that are mainly phloem-fed sink tissues have low Ca-values (Dayod et al. 2010, Hocking et al. 2016). Like parasitic plants, fruits are strong sinks for metabolites and nutrients and the analogous Ca-deficiencies in both tissues are therefore noteworthy. With the ripening process, many fruits (e.g. tomato, apple, kiwifruit and grape) exhibit a dramatic shift in the proportion of xylem and phloem transport, as the contribution of the xylem gradually becomes negligible (Choat et al. 2009, Song et al. 2018). This shift is often accompanied by a sharp drop in Ca uptake (Hocking et al. 2016) and is generally believed to be based on a physical disruption of the fruit xylem or the development of pectin plugs, which reduce the direct hydraulic link of fruit water status to that of the plant (Choat et al. 2009, Hocking et al. 2016). However, new evidence from grapes suggests that ceasing transpiration in ripe fruits leads to a diminishing water potential gradient and this leads to a stop of xylem transport (Chatelet et al. 2008, Choat et al. 2009). Recent work by Keller et al. 2015 even showed that water export, as part of a recycling process to remove surplus water from phloem import, is mediated by a reversal of water flux in the xylem of grape berries (Zhang and Keller 2017). This is an attractive model for the *Cuscuta*-host interaction that may help explain some of the observed mysteries. Adopting this model, we would have to assume that young haustoria, i.e. directly after fusion with the vascular system of the host, would import water and nutrients by both phloem and xylem, which is corroborated by published data (Christensen et al. 2003) and by our ink transport analysis (Fig. 6). In older haustoria, water import by the xylem would be expected to stop or even reverse to remove surplus phloem water that cannot be lost by transpiration in *Cuscuta* due to its low stomata count and lack of leaves. Support for this tentative 'flux reverse model' comes from the observation that proteins (Haupt et al. 2001) or RNA (Kim et al. 2014) can move in both directions over the host/parasite border.

The holoparasitic root parasite *Aeginella indica* (Orobanchaceae), like *C. reflexa*, also exhibits very low Ca levels (2.4 mg g^{-1} dry matter) and low Cl and Mn

concentrations (Watanabe et al. 2007). Interestingly, and in contrast to these two holoparasitic species, the hemiparasite *Odontites verna* (Rozema et al. 1986) that sequesters only inorganic nutrients via xylem connections with their hosts boosts a high accumulation of Ca. Unfortunately, no transpiration rates have been reported for this species, but the high transpiration rates observed in the hemiparasite *Striga*, as a result of the incapacitation of stomatal closure (Fujioka et al. 2019), may hint at the importance of transpiration for the parasite and thus for the Ca-balance and make more detailed comparative studies among parasites imperative.

Author contributions

Conceptualization: I.M., K.F. and K.K. Methodology: F.F., I.M., H.S., K.F. and K.K. Investigation: F.F., I.M., H.S., L.A-M.L., K.F. and K.K. Visualization: F.F., I.M., L.A-M.L., K.F. and K.K.; Figure design, writing and editing: F.F., I.M., B.K., H.S., L.A-M.L., K.F. and K.K. Funding acquisition: B.K. and K.K.

Acknowledgement – We thank Falk Reinhardt (Bruker Nano, Germany) for the first micro-XRF trial measurement and for establishing the interdisciplinary contact between our groups and Eirik Abrahamsen Lænsman for providing the weights of plant samples before and after freeze-drying. This work was supported by grant 16-TF-KK from the Tromsø Research Foundation to K.K., and by grant 152986997 from the German Research Foundation to B.K.

Data availability statement

The data that support the findings of this study are available from the corresponding author upon reasonable request.

References

Andresen E, Peiter E, Küpper H (2018) Trace metal metabolism in plants. J Exp Bot 69: 909–954

Beckhoff B, Kanngießer B, Langhoff N, Wedell R, Wolff H (2007) Handbook of Practical X-Ray Fluorescence Analysis. Springer Verlag, Berlin Heidelberg

Birschwilks M, Haupt S, Hofius D, Neumann S (2006) Transfer of phloem-mobile substances from the host plants to the holoparasite *Cuscuta sp*. J Exp Bot 57: 911–921

Bosch M, Hepler PK (2005) Pectin methylesterases and pectin dynamics in pollen tubes. Plant Cell 17: 3219–3226

de Carvalho GGA, Guerra MBB, Adame A, Nomura CS, Oliveira PV, de Carvalho HWP, Santos D, Nunes LC, Krug FJ (2018) Recent advances in LIBS and XRF for the analysis of plants. J Anal Atom Spectrom 33: 919–944

Chatelet DS, Rost TL, Shackel KA, Matthews MA (2008) The peripheral xylem of grapevine (*Vitis vinifera*). 1. Structural integrity in post-veraison berries. J Exp Bot 59: 1987–1996

Choat B, Gambetta GA, Shackel KA, Matthews MA (2009) Vascular function in grape berries across development and its relevance to apparent hydraulic isolation. Plant Physiol 151: 1677–1687

Christensen NM, Dörr I, Hansen M, van der Kooij TA, Schulz A (2003) Development of *Cuscuta* species on a partially incompatible host: induction of xylem transfer cells. Protoplasma 220: 131–142

Conn S, Gilliham M (2010) Comparative physiology of elemental distributions in plants. Ann Bot 105: 1081–1102

Costea M, Tardif FJ (2005) The biology of canadian weeds. 133. *Cuscuta campestris* Yuncker, *C. gronovii* Willd. ex Schult., *C. umbrosa* Beyr. ex Hook., *C. epithymum* (L.) and *C. epilinum* Weihe. Can J Plant Sci 86: 293–316

Dawson JH, Musselman LI, Wolswinkel P, Dörr I (1994) Biology and control of *Cuscuta*. Rev Weed Sci 6: 265–317

Dayod M, Tyerman SD, Leigh RA, Gilliham M (2010) Calcium storage in plants and the implications for calcium biofortification. Protoplasma 247: 215–231

Doerr I (1969) Feinstruktur intrazellulaer wachsender *Cuscuta*-Hyphen. Protoplasma 67: 123–137

Doerr I (1972) Der Anschluss der *Cuscuta*-Hyphen an die Siebröhren ihrer Wirtspflanzen. Protoplasma 75: 167–184

Etienne P, Diquelou S, Prudent M, Salon C, Maillard A, Ourry A (2018) Macro and micronutrient storage in plants and their remobilization when facing scarcity: the case of drought. Agri 8: 14

Fernando DR, Lynch JP (2015) Manganese phytotoxicity: new light on an old problem. Ann Bot 116: 313–319

Franco-Navarro JD, Brumos J, Rosales MA, Cubero-Font P, Talon M, Colmenero-Flores JM (2016) Chloride regulates leaf cell size and water relations in tobacco plants. J Exp Bot 67: 873–891

de Freitas ST, Handa AK, Wu QY, Park S, Mitcham EJ (2012) Role of pectin methylesterases in cellular calcium distribution and blossom-end rot development in tomato fruit. Plant J 71: 824–835

Fujioka H, Samejima H, Suzuki H, Mizutani M, Okamoto M, Sugimoto Y (2019) Aberrant protein phosphatase 2C leads to abscisic acid insensitivity and high transpiration in parasitic *Striga*. Nature Plant 5: 258–262

Geilfus CM (2018) Chloride: from nutrient to toxicant. Plant Cell Physiol 59: 877–886

Gianoncelli A, Vaccari L, Kourousias G, Cassese D, Bedolla DE, Kenig S, Storici P, Lazzarino M,

Kiskinova M (2015) Soft X-ray microscopy radiation damage on fixed cells investigated with synchrotron radiation FTIR microscopy. Sci Rep 5: 10250
Gilliham M, Dayod M, Hocking BJ, Xu B, Conn SJ, Kaiser BN, Leigh RA, Tyerman SD (2011) Calcium delivery and storage in plant leaves: exploring the link with water flow. J Exp Bot 62: 2233–2250
van Grieken RE, Markowicz AA (2001) Handbook of X-Ray Spectrometry, 2nd Edn. Marcel Dekker Inc, New York
Hänsch R, Mendel RR (2009) Physiological functions of mineral micronutrients (Cu, Zn, Mn, Fe, Ni, Mo, B, Cl). Curr Opin Plant Biol 12: 259–266
Haschke M, Haller M (2003) Examination of poly-capillary lenses for their use in micro-XRF spectrometers. X-ray Spectrom 32: 239–247
Haupt S, Oparka K11J, Sauer N, Neumann S (2001) Macromolecular trafficking between *Nicotiana tabacum* and the holoparasite *Cuscuta reflexa*. J Exp Bot 52: 173–177
Havrilla GJ, Miller T (2004) Micro X-ray fluorescence in materials characterization. Powder Diffr 19: 119–126
Hepler PK (2005) Calcium: a central regulator of plant growth and development. Plant Cell 17: 2142–2155
Hepler PK, Winship LJ (2010) Calcium at the cell wall-cytoplast interface. J Integr Plant Biol 52: 147–160
Hocking B, Tyerman SD, Burton RA, Gilliham M (2016) Fruit calcium: transport and physiology. Front Plant Sci 7: 569
Hongo S, Sato K, Yokoyama R, Nishitani K (2012) Demethylesterification of the primary wall by PECTIN METHYLESTERASE35 provides mechanical support to the *Arabidopsis* stem. Plant Cell 24: 2624–2634
Johnsen HR, Striberny B, Olsen S, Vidal-Melgosa S, Fangel JU, Willats WGT, Rose JKC, Krause K (2015) Cell wall composition profiling of parasitic giant dodder (*Cuscuta reflexa*) and its hosts: a priori differences and induced changes. New Phytol 207: 805–816
Keller M, Zhang Y, Shrestha PM, Biondi M, Bondada BR (2015) Sugar demand of ripening grape berries leads to recycling of surplus phloem water via the xylem. Plant Cell Environ 38: 1048–1059
Kim G, LeBlanc ML, Wafula EK, DePamphilis CW, Westwood JH (2014) Genomic-scale exchange of mRNA between a parasitic plant and its hosts. Science 345: 808–811
Klockenkämper R, von Bohlen A (2015) Total-Reflection X-Ray Fluorescence Analysis and Related Methods. John Wiley & Sons, Hoboken
van der Kooij TAW, Krause K, Dörr I, Krupinska K (2000) Molecular, functional and ultrastructural characterisation of plastids from six species of the parasitic flowering plant genus *Cuscuta*. Planta 210: 701–707
Krause K, Johnsen HR, Pielach A, Lund L, Fischer K, Rose JKC (2018) Identification of tomato introgression lines with enhanced susceptibility or resistance to infection by parasitic giant dodder (*Cuscuta reflexa*). Physiol Plant 162: 205–218
Kuijt J (1969) The Biology of Parasitic Plants. University of California Press, Berkeley
Lachmann T, van der Snickt G, Haschke M, Mantouvalou I (2016) Combined 1D, 2D and 3D micro-XRF techniques for the analysis of illuminated manuscripts. J Anal Atom Spectrom 31: 1989–1997
Liners F, Letesson JJ, Didembourg C, Van Cutsem P (1989) Monoclonal antibodies against pectin: recognition of a conformation induced by calcium. Plant Physiol 91: 1419–1424
Maathuis FJM (2009) Physiological functions of mineral macronutrients. Curr Opin Plant Biol 12: 250–258
Mantouvalou I, Malzer W, Kanngiesser B (2012) Quantification for 3D micro X-ray fluorescence. Spectrochim Acta B 77: 9–18
Mantouvalou I, Lachmann T, Singh SP, Vogel-Mikus K, Kanngiesser B (2017) Advanced absorption correction for 3D elemental images applied to the analysis of pearl millet seeds obtained with a laboratory confocal micro X-ray fluorescence spectrometer. Anal Chem 89: 5453–5460
Neugebauer K, Broadley MR, El-Serehy HA, George TS, McNicol JW, Moraes MF, White PJ (2018) Variation in the angiosperm ionome. Physiol Plant 163: 306–322
Olsen S, Striberny B, Hollmann J, Schwacke R, Popper ZA, Krause K (2016) Getting ready for host invasion: elevated expression and action of xyloglucan endotransglucosylases/hydrolases in developing haustoria of the holoparasitic angiosperm *Cuscuta*. J Exp Bot 67: 695–708
Raven JA (2017) Chloride: essential micronutrient and multifunctional beneficial ion. J Exp Bot 68: 359–367
Rozema J, Broekman R, Arp W, Letschert J, Van Elsbroek M, Punte H (1986) A comparison of the mineral relations of a halophytic hemiparasite and holoparasite. Acta Bot Neerl 35: 105–109
Rydahl MG, Hansen AR, Kracun SK, Mravec J (2018) Report on the current inventory of the toolbox for plant cell wall analysis: proteinaceous and small molecular probes. Front Plant Sci 9: 581
Salt DE, Baxter I, Lahner B (2008) Ionomics and the study of the plant ionome. Annu Rev Plant Biol 59: 709–733
Saric M, Krstic B, Momcilovic V (1991) The relationship of the concentration of mineral elements between host plant (*Pelargonium zonale*) and parasite (*Cuscuta reflexa* ROXB.). Biochem Physiol Pflanzen 187: 105–112
Song WP, Yi JW, Kurniadinata OF, Wang HC, Huang XM (2018) Linking fruit Ca uptake capacity to fruit growth and pedicel anatomy, a cross-species study. Front Plant Sci 9: 575
Storey R, Leigh RA (2004) Processes modulating calcium distribution in citrus leaves. An investigation using x-ray

microanalysis with strontium as a tracer. Plant Physiol 136: 3838–3848
Vaughn KC (2003) Dodder hyphae invade the host: a structural and immunocytochemical characterization. Protoplasma 220: 189–200
Vaughn KC (2006) Conversion of the searching hyphae of dodder into xylic and phloic hyphae: a cytochemical and immunocytochemical investigation. Int J Plant Sci 167: 1099–1114
Wallace A, Romney EM, Alexander GV (1978) Mineral composition of *Cuscuta nevadensis* Johnston (dodder) in relationship to its hosts. Plant and Soil 50: 227–231
Watanabe T, Broadley MR, Jansen S, White PJ, Takada J, Satake K, Takamatsu T, Tuah SJ, Osaki M (2007) Evolutionary control of leaf element composition in plants. New Phytol 174: 516–523
Wege S, Gilliham M, Henderson SW (2017) Chloride: not simply a 'cheap osmoticum', but a beneficial plant macronutrient. J Exp Bot 68: 3057–3069
White PJ, Broadley MR (2009) Biofortification of crops with seven mineral elements often lacking in human diets – iron, zinc, copper, calcium, magnesium, selenium and iodine. New Phytol 182: 49–84
White PJ, Broadley MR, El-Serehy HA, George TS, Neugebauer K (2018) Linear relationships between shoot magnesium and calcium concentrations among angiosperm species are associated with cell wall chemistry. Ann Bot 122: 221–226
Willats WGT, Orfila C, Limberg G, Buchholt HC, van Alebeek GJWM, Voragen AGJ, Marcus SE, Christensen TMIE, Mikkelsen JD, Murray BS, Knox JP (2001) Modulation of the degree and pattern of methyl-esterification of pectic homogalacturonan in plant cell walls – implications for pectin methyl esterase action, matrix properties, and cell adhesion. J Biol Chem 276: 19404–19413
Zhang Y, Keller M (2017) Discharge of surplus phloem water may be required for normal grape ripening. J Exp Bot 68: 583–593

Supporting Information

Additional supporting information may be found online in the Supporting Information section at the end of the article.

Fig. S1. Element composition of extracts from apical shoot tips of *Cuscuta reflexa*.

Fig. S2. Impact of sample preparation, stem age and stem type on element spectrum intensity and relative amounts.

Fig. S3. Element distribution in *Cuscuta reflexa* infection sites.

Fig. S4. Elemental distributions in infection sites of *Cuscuta reflexa* on two different hosts, *Pelargonium zonale* and *Pelargonium citriodorum*.

Fig. S5. Immunological detection of calcium-crosslinked pectin.

Movie S1. Video file showing a rotating confocal 3-D representation of the scanned area shown in Fig. 4B.

Edited by J. Schjørring